

Test and sensitivity analysis of base-isolated steel frame with low-friction spherical sliding bearings

Motoki Akazawa¹ | Masahiro Kurata²  | Shinsuke Yamazaki³ |
Yohsuke Kawamata⁴ | Shintaro Matsuo⁵

¹Takenaka Corp, Osaka, Japan

²Disaster Prevention Research Institute, Kyoto University, Kyoto, Japan

³Nippon Steel Engineering Co., Tokyo, Japan

⁴National Research Inst. for Earth Science and Disaster Resilience, Hyogo, Japan

⁵Department of Architecture and Urban Design, Kyushu University, Fukuoka, Japan

Correspondence

Masahiro Kurata, Disaster Prevention Research Institute, Kyoto University, Kyoto, Uji 611-0011, Japan.
Email: kurata.masahiro.5c@kyoto-u.ac.jp

Funding information

Tokyo Metropolitan Resilience Project of the National Research Institute for Earth Science and Disaster Resilience (NIED); Japan Society for the Promotion of Science, Grant/Award Number: JP21H04598

Abstract

In Japan, spherical sliding bearings with low friction coefficients are gaining popularity for base-isolating low-rise frames that are relatively lightweight. However, the complete dataset of isolators and a base-isolated frame for evaluating the model sensitivity and response uncertainty are limited. This study first presents the design process, isolation unit- and frame-level testing, and a blind prediction contest conducted on the occasion of full-scale shaking table testing of a three-story base-isolated hospital specimen. The design process utilizes a numerical model that accounts for the velocity and contact pressure dependencies and requires soft- and hard-case simulations with nominal friction coefficients plus and minus standard deviation to consider the uncertainties associated with the bearing behavior. The pre-shipment isolation unit and frame shake table testing yielded an invaluable dataset for bearings under normal and low contact pressures, low and high velocities, and constant and varying axial loads. The accompanying blind prediction contest provided a valuable dataset for rethinking the impact of modeling uncertainty. In-depth data analysis and sensitivity analysis were conducted. The sliding coefficient increased under low-contact pressure and low-velocity conditions. The static friction coefficient was 1.9 to 4.5 times higher than the dynamic coefficient, but this had little impact on the residual displacement, cumulative travel, and maximum story shear force. The axial force fluctuation, vertical motion, and two-directional input did not significantly affect the bearing behavior in the test. The test and the following simulations confirmed that the low friction coefficient helped the building contents, that is, medical equipment in this study, remain in order under near-fault and long-period ground motions.

KEYWORDS

medical equipment, seismic isolation, shake table testing, sliding coefficient, spherical sliding bearing, velocity dependency

This is an open access article under the terms of the [Creative Commons Attribution-NonCommercial-NoDerivs](https://creativecommons.org/licenses/by-nc-nd/4.0/) License, which permits use and distribution in any medium, provided the original work is properly cited, the use is non-commercial and no modifications or adaptations are made.

© 2024 The Author(s). *Earthquake Engineering & Structural Dynamics* published by John Wiley & Sons Ltd.

1 | INTRODUCTION

The number of base-isolated buildings has steadily increased in Japan, where significant ground motions induced by large near-fault earthquakes or subduction zone mega-earthquakes are highly probable.¹ Medical facilities are a type of building in which the application rate of seismic isolation has been increasing. During the 2016 Kumamoto earthquake with $M_j7.3$ ($M_w7.0$), hospitals located in areas with a seismic intensity of less than six or more than five on the Japanese Meteorological Agency scale underwent evacuation, which interrupted inpatient care and significantly affected local medical care.² Kumamoto University Hospital, located at a site with less intensity, still reported damage to furniture and laboratory contents in buildings diagnosed as earthquake-resistant, but base-isolated buildings experienced no impact. In the 2023 Kahramanmaraş earthquake sequence, base-isolated hospitals became fortresses for earthquake-affected areas. In Turkey, base isolation has been mandatory for hospitals with more than 100 beds in high-seismic zones since 2013. Such incident reports considerably influence the medical community's incentives to choose base isolation techniques.

Hospital owners and medical staff expect outstanding seismic performance in base-isolated buildings with negligible or no impact on building usage. This overconfidence leads to incorrect decisions regarding earthquake preparedness in base-isolated hospitals. Sato et al. conducted a quantitative evaluation of the vulnerability of medical equipment to earthquake damage by placing medical equipment in two types of seismically isolated buildings, one with natural laminated rubber and steel dampers and the other with high-damping laminated rubber and an intrinsic period of approximately 2.5 s, as full-scale buildings simulating the early days of seismic isolation.³ The study observed very high medical function retention for short-period ground motions but massive movement of caster equipment and fatal damage for long-period ground motions.^{4–8} This observation suggests that the earthquake engineering community should continue examining the relationship between isolators' characteristics and the damage prediction of building contents.^{9–13}

Friction pendulum bearings (FPBs) are gaining popularity in Japan for base-isolating low-rise frames, gymnasium roofs, and facilities, which are relatively lightweight. An FPB is a seismic isolation system in which a slider with a Teflon surface is installed on a steel sphere known as a concave plate for sliding.¹⁴ The maximum deformation could be adjusted according to the diameter of the concave plate. While laminated rubber bearings have difficulty achieving the deformation capacity and extended period with a low axial force, the FPB realizes the extended natural period of the isolated frame independently of the support weight. FPB has a restoring mechanism based on the pendulum motion and a historical damping mechanism using frictional forces. Compared with the limited applications in Japan, the research and application of FPBs have a long history outside of Japan, including failure analysis against extreme motions.¹⁵ The relevant literature can be found elsewhere.

More recently, FPBs with low friction coefficients, called low-friction spherical sliding bearings (LF-SSBs), have been introduced in the Japanese market to reduce the acceleration response of superstructures further. A conventional SSB uses polytetrafluoroethylene double-woven fabric as the sliding material and a stainless-steel sliding plate with a mirror finish. The LF-SSB achieved a friction coefficient of 0.013 by impregnating a sliding material with a lubricant. In general, sliding bearings exhibit velocity and contact pressure dependencies.¹⁶ Under a low-friction condition, the friction coefficient variations under low contact pressure and low velocity become notable.¹⁷ Moreover, the static friction coefficient, generally larger than the sliding friction coefficient, is not specified as a design value.^{18,19} The effects of these variations on the responses of superstructures and their contents have not been thoroughly investigated, and there is no shaking-table testing data for frames isolated with full-scale LF-SSBs.

This study examined the effects of the contact pressure, velocity, and static friction coefficients on the performance of LF-SSBs through the isolation unit testing of the isolators and the shaking table test of a full-scale hospital specimen at an E-Defense facility. Pre-shipment dynamic tests on the isolation devices yielded a dataset to check the manufacturing variability, velocity dependency, and contact pressure dependency. The full-scale base-isolated frame was tested under near-fault and long-period ground motions. As a part of the testing campaign, a blind prediction contest was conducted, and variations in prediction results were evaluated. With a numerical simulation model prepared initially for design, the response prediction accuracy using the design equations was examined, addressing the design tips to predict the behavior accurately at low-pressure conditions. Finally, the impact of sliding coefficients on the behavior of building content, that is, medical components in this study, are discussed.

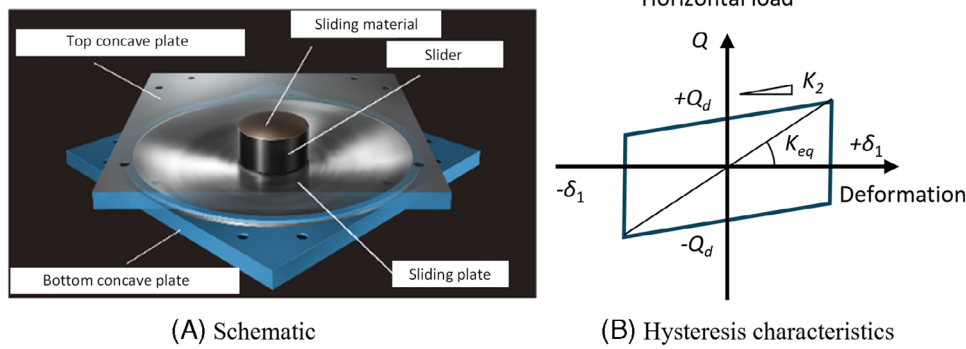


FIGURE 1 Spherical sliding bearing (friction pendulum).

2 | CHARACTERISTICS OF LOW-FRICTION SPHERICAL SLIDING BEARINGS

2.1 | Uncertainty considered in design

The seismic isolation system considered in this study is an LF-SSB system. Figure 1A shows a schematic of the seismic isolation device. The SSB consists of concave spherical sliding plates above and below the moving body called a slider. The upper and lower surfaces of the slider have PTFE material as a sliding material. For LF-SSB, the PTFE material is impregnated with a lubricant for the low-friction specification with a nominal coefficient of friction of 0.013.

Figure 1B shows the idealized bilinear characteristics of the hysteresis characteristics.²⁰ After overcoming the dynamic slip-resistance load Q_d , the slider starts to slide and has a horizontal secondary stiffness K_2 . The nominal natural period of the base-isolated structure is computed using K_2 , whereas the actual natural period depends on the equivalent stiffness K_{eq} , which also depends on the sliding displacement.

In the design of LF-SSBs, manufacturing variations and variations caused by velocity, cyclic pressure, and contact pressure dependencies must be considered. The following equations can be used to calculate the dynamic slip resistance load and horizontal secondary stiffness.

$$Q_d = \tau_q \cdot \mu \cdot P \quad (1)$$

where τ_q is the coefficient of variation, μ is the coefficient of friction, and P is the vertical load.

$$K_2 = P / (2 \cdot R_s) \quad (2)$$

where R_s is the spherical radius of the concave sliding plate.

The coefficient of variation is computed by the product of contact pressure dependency, X , velocity dependency, γ , and cyclic dependency, C . The formulae for these dependencies are given in Equations (3)–(5), respectively.

Contact pressure dependency,

$$X = 20 \cdot \sigma^{-0.9} + 0.5 \quad (3)$$

Velocity dependency

$$\gamma = 1.03 - 0.55 \cdot 1.5^{-0.018V} \quad (4)$$

Cyclic dependency

$$C = -0.05 \quad (5)$$

where σ is the contact pressure, and V is the Velocity.

TABLE 1 Loading protocol.

Test method	Control wave	Axial force	Test velocity	Amplitude
Constant-amplitude	Sine wave	60 MPa	20 mm/s	± 50 mm
cyclic		30 MPa, 60 MPa	400 mm/s	± 200 mm

The standard contact pressure of the LF-SSB is 60 MPa, and the minimum contact pressure recommended by the manufacturer is 30 MPa. The contact pressure dependency equation shows that Q_d increases by 43% from the standard application when the contact pressure is at the specified minimum (3). When the sliding velocity increases from 100 to 400 mm/s, Q_d increases by 33.5%, according to the velocity dependency Equation (4).

2.2 | Base isolation unit testing

LF-SSB is a ministry-certified device. In the certification process, experts from a third-party inspection organization confirm that the seismic isolation materials have the performance specified in the manufacturer's application and that the quality control system of the manufacturing plant is implemented as described in the certification application. In Japan, LF-SSBs require product acceptance inspections of standard quasi-static tests before shipping for all the devices (full inspection).

All four seismic isolators prepared for the shaking table test of a full-scale building specimen required quasi-static testing for the inspection process. In addition, this study conducted dynamic tests to evaluate the influence of sliding velocity.

2.2.1 | Testing machine properties

The testing machine accommodated quasi-static and dynamic loadings. In the quasi-static mode, the machine had a maximum vertical load of 22,000 kN and a maximum horizontal load of 2000 kN. In the dynamic mode, the machine had a maximum vertical load of 2000 kN, a maximum horizontal load of ± 200 kN, and a maximum horizontal velocity of 400 mm/s.

2.2.2 | Loading protocols

The loading protocol, certified for the LF-SSB, consisted of four cycles of constant-amplitude sine waves with a contact pressure of 60 MPa and a maximum loading velocity of 20 mm/s. In addition to the quasi-static loading, dynamic loading was added to evaluate the constant pressure and velocity dependency. Table 1 summarizes the loading conditions. The selected contact pressures were 30 and 60 MPa, and the selected maximum velocities were 20 and 400 mm/s. The selected loading amplitudes were ± 50 mm for the maximum velocity of 20 mm/s and ± 200 mm for the maximum velocity of 400 mm/s. For each test, the loading was repeated for four cycles.

Following a standardized procedure, the hysteresis behavior in the third cycle was evaluated to obtain the friction coefficients. Table 2 shows the test results, and Figure 2 shows the results plotted against the manufacturer's previous experiments and the predictions obtained using the dependency equations.

Under the dynamic loading conditions of 400 mm/s and a standard contact pressure of 60 MPa, the average friction coefficient of the four isolators was 0.0106. The results vary from a nominal value of +0.013% to -18.4%.

When the loading velocity decreased to the standard quasi-static loading condition of 20 mm/s, the average friction coefficient of the four isolators was 0.0126. The result was 1.19 times larger than the average friction coefficient of 0.0106 at 400 mm/s. In Figure 2A, the result is 34.6% larger than the value predicted using the velocity dependency Equation (4). When the contact pressure was reduced to 30 MPa, the average friction coefficient was 0.0179, 1.69 times larger than that at 60 MPa (0.0106). Figure 2B shows the result is 17.8% larger than the value predicted using the contact pressure dependency Equation (3).

The test results showed that the friction coefficients under low-velocity loading increased significantly compared with those predicted using the recommended equations. Thus, this study developed the new velocity dependency equation, γ' ,

TABLE 2 Isolation unit testing results of LF-SSB.

No.	Contact pressure P (MPa)	Temp. T (°C)	Velocity V (mm/s)	Friction Coeff. (F.C.) corrected for 20°C, 400 mm/s, 60 MPa μ	F.C. variation from design value %	Average Ave (μ)
60_400_1	60	21.3	400	0.0111	-14.3	0.0106
60_400_2	60	21.8	400	0.0116	-10.5	
60_400_3	60	21.9	400	0.0101	-22.4	
60_400_4	60	21.6	400	0.0096	-26.5	
60_20_1	60	21.0	20	0.0125	-3.7	0.0126
60_20_2	60	21.3	20	0.0132	1.3	
60_20_3	60	21.5	20	0.0121	-7.3	
60_20_4	60	21.3	20	0.0128	-1.6	
30_400_1	30	20.8	400	0.0171	31.5	0.0179
30_400_2	30	21.4	400	0.0200	54.1	
30_400_3	30	21.5	400	0.0186	43.0	
30_400_4	30	21.3	400	0.0160	22.7	

Abbreviation: LF-SSB, low-friction spherical sliding bearings.

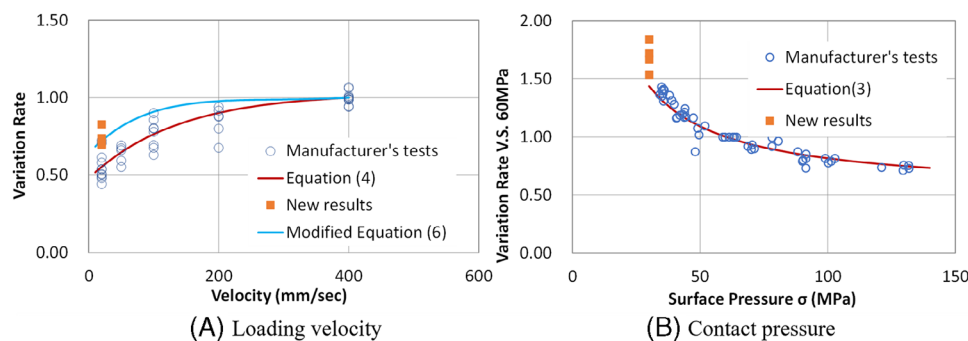


FIGURE 2 Change in coefficient of friction owing to contact pressure and loading velocity.

(6) via regression analysis of the present elemental experimental results.

$$\gamma' = \left(1.03 - 0.55 \cdot 1.5^{-0.018V}\right) \cdot \left(\frac{0.336}{400^2} \cdot (V - 400)^2 + 1\right) \quad (6)$$

3 | FULL-SCALE SHAKING TABLE TESTING

3.1 | Specimen

The specimen was a three-story frame with a one-by-one plan. In Japanese design practice, seismic response analysis is performed for earthquakes that occur extremely rarely (approximately 500 years return period), and allowable stress design is performed for the shear forces obtained from the analysis. For the test specimen, the allowable stress design was performed for a base shear factor of 0.2, since the base shear factor obtained from the seismic response analysis was less than 0.2. Figure 3A shows the specimen installed on the shaking table. The base-isolated specimen was then placed on the right side. For comparison, an earthquake-resistant four-story frame specimen, named fixed-base specimen, was installed on the left side, and the two frames were connected to the second floor by an expansion joint. Since the expansion joint functioned adequately, the effect of the response of the fixed-based specimen was assumed to be negligible in the experimental results.

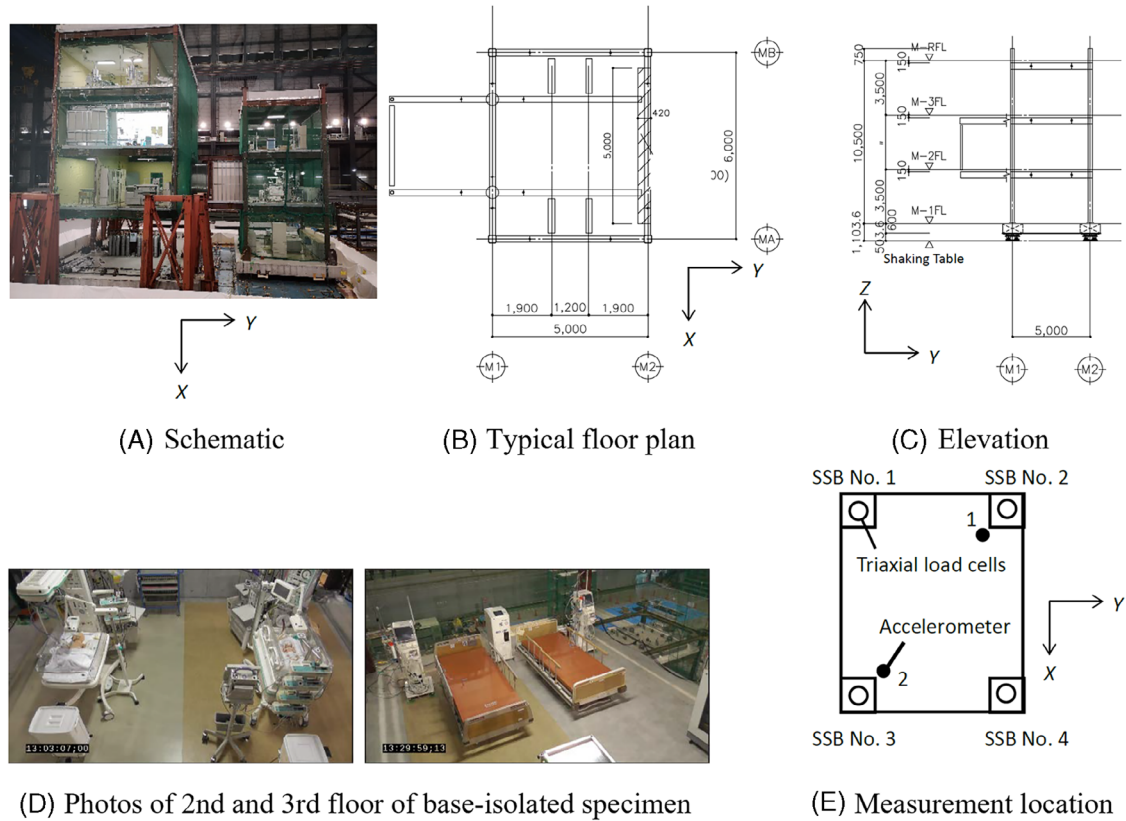


FIGURE 3 Specimen.

TABLE 3 Cross-section of structural members (unit: mm).

Member	Dimensions	Material Type
Columns	HSS-250 × 250 × 9	BCR295 ($\sigma_y = 295$ MPa)
Beams	H-400 × 200 × 8 × 13	SN490B ($\sigma_y = 325$ MPa)
Foundation beams	1500 (width) × 600 (depth)	RC, $F_c' = 24$ MPa
Slab	$t = 150$	RC, $F_c' = 36$ MPa

Figure 3B,C show the floor plan and elevation of the base-isolated specimen, respectively. The floor plan is 6.0 m × 1 span in the long (X) direction, 5.0 m × 1 span in the short (Y) direction, and the height is approximately 12 m with an aspect ratio of approximately 2. The second floor had a 3.0-m-long overhang as a corridor connected to the earthquake-resistant specimen through an expansion joint. Weight-adjusting masses were installed on the first and second floors to prevent eccentricity. Table 3 presents the cross-sections and steel types of the main members. The frame consists of cold-formed square steel tube columns and H-shaped steel beams. The foundation beams had a width of 1500 mm and a depth of 600 mm, and the first-floor slab had a thickness of 600 mm. The second and third-floor slabs had a thickness of 150 mm. The roof was 600 mm thick to increase the mass of the specimen.

The specimens were designed as hospitals and thus had various types of medical equipment in each room. Figure 3D shows the room arrangement for the NICU (Neonatal Intensive Care Unit) on the second floor and the dialysis treatment room on the third floor. Most of the equipment contained casters. Most equipment casters were locked or half-locked.

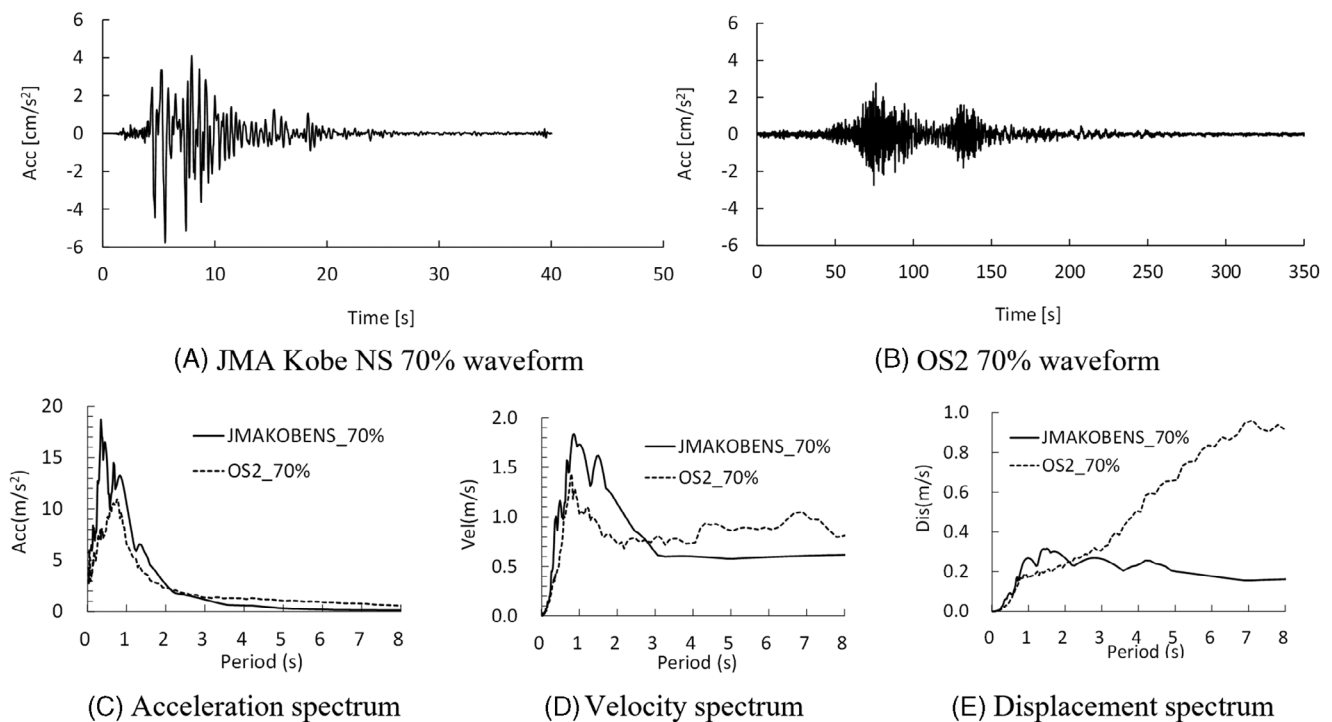
3.2 | Measurement plan

Each isolator was supported by four triaxial load cells to measure the vertical and horizontal loads applied to the isolator (Figure 3E). Laser displacement transducers were used to measure the vertical and horizontal displacements at two

TABLE 4 Loading and observation schedule.

ID	Input motion	Evaluated performance
1, 2	JMA Kobe NS <i>X</i> dir. 16%; <i>Y</i> dir. 16%	Elastic limit
3	OS2 <i>Y</i> dir. 20%	Elastic limit, long period, and duration
4 ^a	JMA Kobe NS <i>X</i> dir. 50%	Ultimate strength limit
5 ^a	OS2 XY 45° (<i>X</i> + <i>Y</i> dirs.) 70%	Ultimate strength limit, long period, and duration
6 ^a	JMA Kobe NS 45° (<i>X</i> + <i>Y</i> dirs.) 70%, UD <i>Z</i> dir. 100%	Above design level

^aObservation inside the specimen after loading.

**FIGURE 4** Input earthquake motions.

diagonal locations on the first floor. Three-axis accelerometers were installed at two diagonal locations on each floor. The actual loads were measured by using triaxial load cells. After the trial installation, steel shim plates were inserted to uniform the loads supported by the isolators. The total weight of the specimen was 1873 kN, including the contents, and the average contact pressure was 26.5 N/mm². The identified natural period of the superstructure in non-sliding conditions was 0.71 s in both the *X* and *Y* directions.

3.3 | Loading schedule

JMA Kobe NS and OS2 were used for excitation. JMA Kobe NS is the observed earthquake ground motion during the Hyogo-ken Nanbu earthquake, and OS2 is the simulated design long-period earthquake ground motion for the Nankai Trough. OS2 provided for the engineering bedrock was amplified by assuming a normal soil type. Table 4 lists the input motions, scales, input directions, and timing of the observations after each excitation. The excitation level is expressed as a factor (%) of acceleration relative to the original wave. Figure 4 shows the acceleration time history and acceleration, velocity, and displacement response spectra for the JMA Kobe NS in 70% scale for 45° (*X* + *Y* directions) and OS2 XY in 70% scale for 45° (*X* + *Y* directions), respectively. JMA Kobe has a strong power in the short-period range, but in the 2.5 s or longer range, OS2 outpowers JMA Kobe.

TABLE 5 Maximum responses, $\mu_0 = 0.013$.

Floor acceleration (unit: cm/s^2)						
ID	1	2	3	4	5	6
3rd Floor	95.6	90.7	82.7	89.3	172	130
2nd Floor	79.3	66.3	52.5	91.7	114	115
1st Floor	79.8	63.7	46.0	79.8	131	101
Table	120	136	74.5	357	283	529
Floor velocity (unit: cm/s)						
3rd Floor	10.0	10.9	10.9	16.8	25.9	19.5
2nd Floor	9.58	10.0	8.08	17.6	24.4	19.0
1st Floor	9.41	9.45	9.17	15.3	24.6	17.2
Table	14.9	15.0	10.1	45.9	31.5	63.2
Base isolation layer response displacement (unit: cm)						
1st Floor	2.48	3.16	2.83	11.2	18.6	15.2

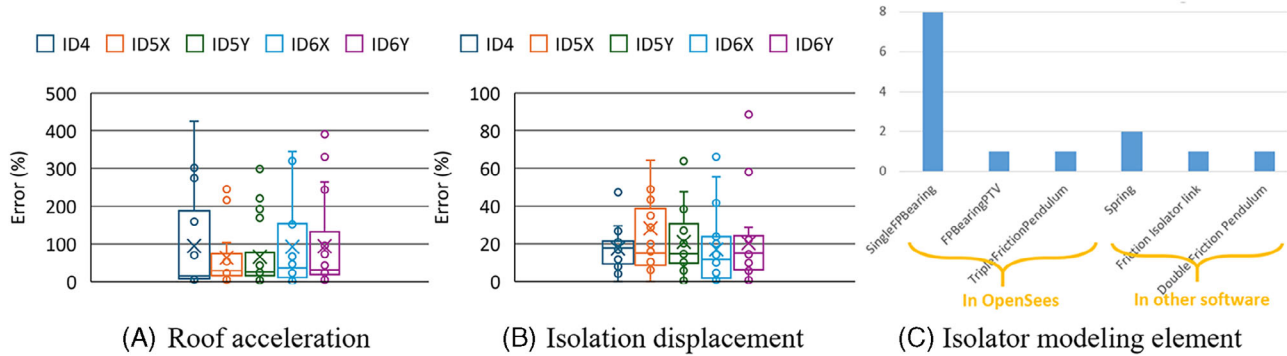


FIGURE 5 Blind prediction contest results.

3.4 | Maximum responses

The maximum acceleration, velocity, and displacement of the seismic isolation layer for each floor under each excitation are summarized in Table 5. The maximum floor response acceleration, floor response velocity, and displacement of the base isolation layer were 172 cm/s^2 , 26 cm/s , and 19 cm for ID5, respectively. The shaking table's acceleration and velocity were approximately twice as high in ID6 than in ID5, which was considered reasonable because OS2 was also larger in the response spectrum above 3.0 s. The interstory drift of the superstructure remained far below its elastic limit.

3.5 | Blind-prediction contest results

The testing also presented an opportunity to host a multi-phase Blind Prediction Competition (BPC) to examine the current integrated structural/nonstructural modeling capability. Students, researchers, and practicing engineers participated in this competition. The results helped identify areas of uncertainty and determine current, reliable modeling techniques while pinpointing future research opportunities. Contestants were invited to participate as teams or individuals, with students, researchers, and professionals encouraged to participate. The contestants could use commercial or non-commercial software for their analysis. All participants were provided with building drawings, a design catalog with the nominal values and the equations for surface and velocity dependencies, and isolation unit testing data (results summarized in Table 2). Results were submitted and assessed through a provided spreadsheet and a one-page summary of the numerical approach.

Figure 5 shows the box-and-whisker plot of the error of the submitted results over the test results. There were seventeen valid submissions and one invalid submission. The prediction accuracy was better for roof acceleration over isolation displacement. The average errors on the roof acceleration peaks over the test are around 65%–93%, depending on test IDs,

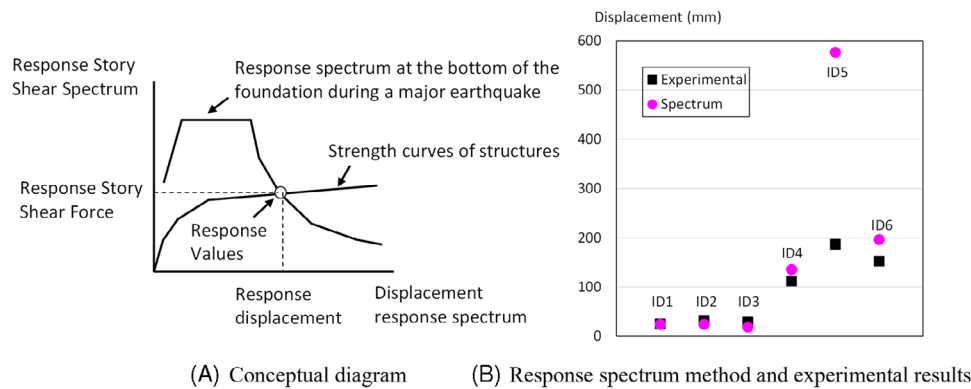


FIGURE 6 Prediction using the response spectrum method.

while the error on the isolation displacement is 17%–28%. Ten teams utilized OpenSees, four utilized other software, and three did not describe the software name. In OpenSees, most teams utilized singleFPBearing element. The top-performing team, one student from China, had 10.3% and 8.9% errors for roof acceleration and isolation displacement using OpenSees with the singleFPBearing element.

4 | RESPONSE PREDICTION AND SOURCE OF UNCERTAINTY

4.1 | Response prediction using response spectrum method

The response spectrum method is a typical method that is simpler than the time-history response analysis for evaluating the seismic response of seismically isolated buildings.²¹ This method uses the response spectrum of the input earthquake motion to obtain the maximum response according to the hysteresis characteristics of the seismic isolation layer. It has been implemented in Japan through guidelines and regulations.²² However, its scope of application is limited. This method does not apply to buildings over 60 m in height or the structural type of intermediate seismic isolation. Furthermore, its effects on long-period ground motion have not been verified.

The concept of response evaluation using the response spectrum method is described. This method uses the response spectrum based on the equivalent linearization method, whose concept is shown in Figure 6A. The vertical axis represents the product of the response acceleration and mass, and the horizontal axis represents the response displacement. The story shear force and displacement response pairs were plotted as a response spectrum at a certain period. The strength curve of the base-isolated system is estimated by manufacturing variation and contact pressure dependence from isolation unit testing. The intersection point obtained by superimposing these two values was the response value. Since the equivalent damping ratio, H_{eq} , of the seismic isolation layer at the response displacement was used to construct the response spectrum; a convergence calculation is required to obtain the true response value. The equivalent damping ratio, H_{eq} , was 11%~28% in this calculation.

Figure 6B compares the experimental results of ID1–6 with the response values predicted using the response spectrum method, assuming that the earthquake ground motion level is a medium earthquake or higher. The bearing capacity curve of the spherical sliding bearing considers the manufacturing variation and contact pressure dependence obtained from the isolation unit tests. The predicted values for the JMA Kobe motion generally correspond well to the experimental results of ID1, 2, 4, and 6. However, for long-period earthquake motion, the response spectrum method shows an excessively large value compared with the experimental results of ID5, whereas there is a good correspondence for ID3.

4.2 | Numerical analysis model

For the seismic response analysis, the three-dimensional frame model shown in Figure 7A was used as the basis. To verify the effects of the fluctuating axial and two-directional applied forces on the numerical analysis, a multi-degree-of-freedom (MDOF) model (Figure 7B), which is a lumped mass model generally used in the design of seismically isolated buildings,

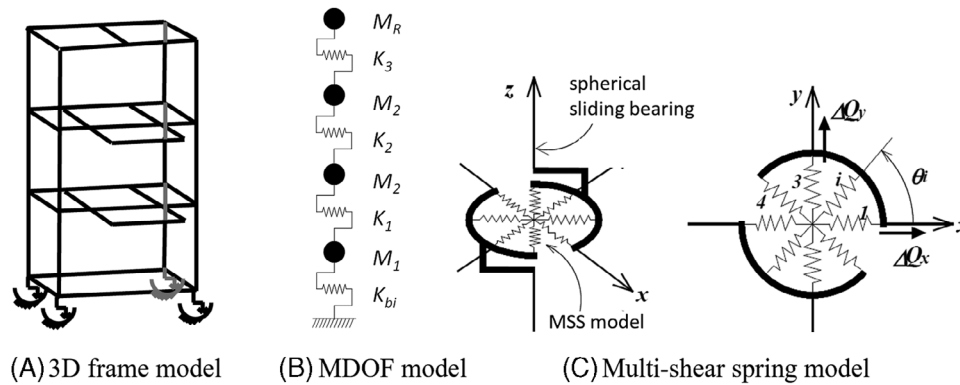


FIGURE 7 Numerical analysis model.

was also used. The axial forces acting on the seismic isolator under long-term loading were equivalent to the experimental and numerical analysis values. A general-purpose structural analysis software called SNAP was used for simulations.

The spherical sliding bearing was modeled using a multi-shear spring model, commonly used in Japanese design practice. A multi-shear spring model simulates the behavior of column members subjected to shear stress from multiple directions. The model consists of multiple springs arranged isometrically in the central section of the column (Figure 7C). Each spring bears a shear deformation and shear force in each direction. In this study, the shear springs of the multi-shear spring model are arranged in eight directions, including x and y axes.

In this study, the isolation unit tests of the SSB were conducted before the E-Defense experiment, as described in Section 2. Thus, the modeling of the seismic isolation system in the numerical analysis considered the results of the isolation unit tests as follows:

1. For the variation in the friction coefficient owing to manufacturing variations, the ratio of the average value of the isolation unit test results to the catalog value was multiplied by the dynamic sliding resistance Q_d .
2. For the variation in the friction coefficient owing to the contact pressure dependence, the coefficient of variation of 30 MPa/60 MPa was 1.178 times higher than the manufacturer's catalog value according to the results of the isolation unit tests, and this value was multiplied by Q_d .
3. Regarding the variation in the friction coefficient owing to velocity dependence, the results of the isolation unit tests conducted by the manufacturer showed that the variation was large, even below 200 mm/s. In the isolation unit tests conducted in this study under 20 mm/s loading conditions, the variation was +33.6% compared with reference.¹⁷ Two models were used to confirm the effect of this variation on the behavior at low velocities: the manufacturer's recommended Equations (4)–(6) modified based on the isolation unit tests.

The relationship between the displacement of the seismic isolation layer and the natural period of the system was verified through numerical analysis. The equivalent natural period of the system was 4 to 5 s at the response displacement of 100 to 400 mm for a medium to large earthquake. In the small displacement range of the response to small earthquakes, the equivalent natural period of the system was smaller than 4 s.

4.3 | Velocity dependency

The dynamic sliding resistance load of the LF-SSB fluctuates with velocity in the low-velocity range, as shown in Figure 2. Therefore, an appropriate evaluation of the velocity dependence at low velocities is essential for predicting accurately the displacement and story shear force responses. This section examines how well the numerical analysis and the experimental results correspond to each other.

For the numerical simulation, the modified Equation (6) based on the isolation unit test and Equation (4) for the velocity dependence recommended by the manufacturer were first compared. The values computed by Equation (4) were 1.24, 1.08, and 1.19 times those by Equation (6) for ID2, ID4, and ID5, respectively. The average velocity during the primary sliding period, described in Section 4.5.2, was used for calculation.

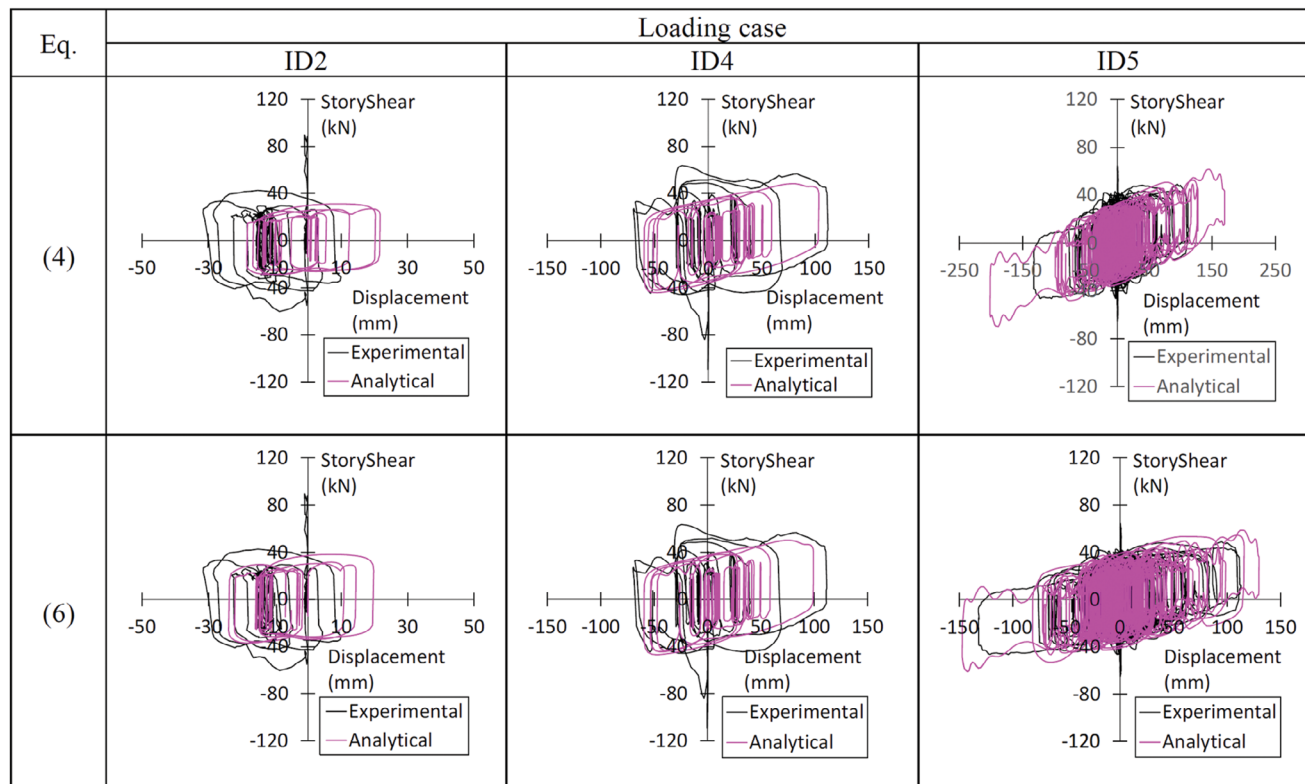


FIGURE 8 Hysteresis characteristics of the base isolation layer.

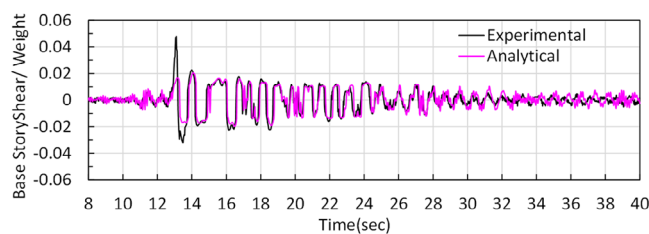


FIGURE 9 Time-history response of story shear force/total weight (ID2).

Figure 8 shows the hysteresis characteristics of the experimental and numerical results of the seismic isolation layers for ID2, ID4, and ID5 using the proposed Equation (6). In the case of ID4, where the maximum velocity was approximately 400 mm/s, there was no significant effect on the behavior of the maximum response between the experimental and numerical results, and the experimental results could be evaluated accurately. For a low velocity, such as in the case of ID5, where the maximum velocity was approximately 300 mm/s, the difference in the maximum response displacement between the two equations is noticeable. Furthermore, by using modified Equation (6) for the isolation unit tests, there is a good correspondence between the experimental and numerical analysis results, confirming the validity of the proposed numerical analysis model. In the cases of ID4 and ID5, for the initial motion, the experimental results showed a large value of the base isolation layer shear force owing to the effect of the static friction coefficient, which was not considered in the numerical analysis, confirming the discrepancy in the timing during sliding between the numerical analysis and the experimental results.

For a small input acceleration in the case of ID2, the maximum response displacements predicted using both equations differed from the experimental results because of the large effect of the static friction coefficient on the initial motion. Figure 9 shows the effect of the static friction coefficient on the time history response of the story shear force normalized by the total weight. The isolation unit test modified in Equation (6) corresponded well with the test results when focusing on the story shear force/total weight after 14 s. Thus, it is necessary to consider the increase in the friction coefficient as a velocity-dependent equation in the design under a low contact pressure and velocity.

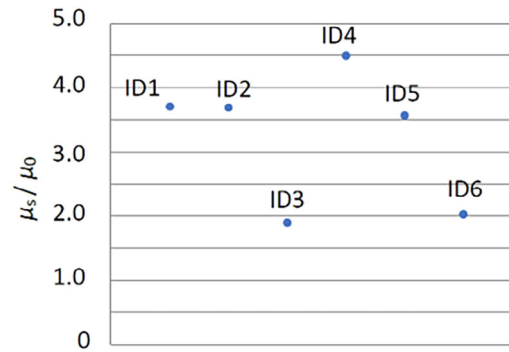


FIGURE 10 Amplification of static friction coefficient.

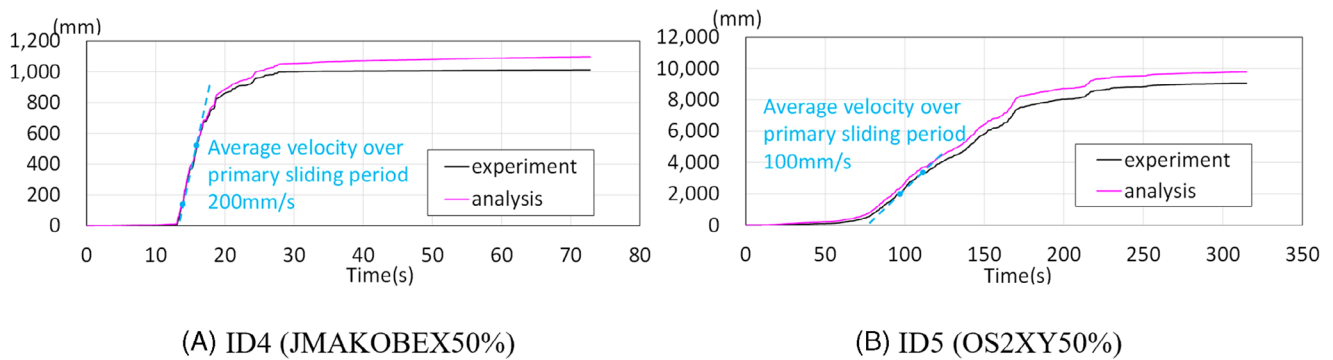


FIGURE 11 Cumulative travel.

4.4 | Static friction

4.4.1 | Magnitude of static friction

The static friction coefficient was larger than that of dynamic friction. However, its effect on the maximum response was considered to be small because it was limited to the initial motion. Therefore, it was not evaluated quantitatively and was not considered in the current design. In this study, the effects of the static friction coefficient on each excitation were examined, including the magnitude of the static friction coefficient, the effect of the static friction coefficient on the time displacement and cumulative travel of the base isolation layer, the effect of the static friction coefficient on the residual displacement, and the effect of the static friction coefficient on the behavior of the superstructure. The coefficient of static friction μ_s in this paper is defined as the maximum shear force of the base-isolation layer divided by the overall weight before the start of the slide.

Figure 10 shows the magnitude of the static friction coefficient for each excitation. The horizontal axis shows each excitation case number, and the vertical axis shows the coefficient of static friction μ_s divided by the nominal coefficient of dynamic friction $\mu_0 = 0.013$. The static friction coefficient was 1.9 to 4.5 times higher than the dynamic coefficient and its average of $\mu_s = 0.042$ was 2.3 times higher than the isolation unit testing results of 0.0179 listed in Table 2

4.4.2 | Impact on cumulative travel

Figure 11 compares the cumulative sliding distance in the experiments and numerical analysis for ID4 and ID5, respectively. In ID4, the difference in the cumulative sliding distance between the numerical analysis and experimental results was 84 mm, approximately 8% of the total sliding distance of 1096 mm. In ID5, the difference was 733 mm, approximately 8% of the total sliding distance of 9779 mm. As mentioned in Section 4.3, the sliding timing differed from the experimental

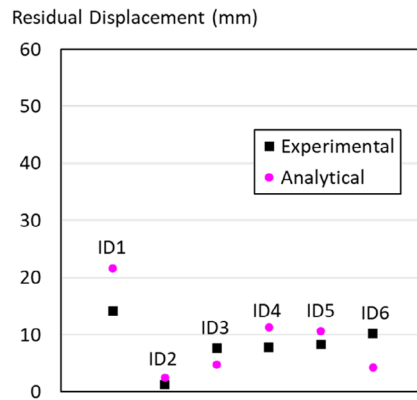


FIGURE 12 Residual displacement.

results to the numerical analysis, likely because the numerical analysis did not consider the effect of the static friction coefficient. However, the difference in the timing of sliding had a negligible effect on the cumulative travel.

The plots also show an interesting fact on the average velocities over the primary sliding period, which were 200 mm/s and 100 mm/s for ID4 and ID5, respectively. The sliding velocity was twice from JMAKOBEX to OS2 motion. Note that the velocity spectrum shown in Figure 4D is larger for JMAKOBEX than OS2 in the natural period range from 0.8 to 2.8 s.

4.4.3 | Impact on residual displacement

In Japan, the maintenance design guideline of the Japan Society of Seismic Isolation²³ specifies the allowable residual displacement as 50 mm, and the concave radius of LF-SSB is designed to meet the specification. In design, seismic response analysis is continued after input motion terminates, and the residual displacement is evaluated under free vibration.

Figure 12 shows the residual displacement of the seismic isolator for each loading case. The horizontal axis represents the loading case number, and the vertical axis represents the residual displacement of the seismic isolator. In both the experimental and numerical results, the residual displacement was less than 50 mm for both cases. In addition, the residual displacement was largest for ID1 (JMAKOBEX16%) in both the experiment and numerical analysis. However, there was almost no residual displacement for ID2 (JMAKOBEX16%), which had the same input acceleration but a different input direction.

4.4.4 | Impact on frame responses

Figure 13 illustrates the time-history displacement and story shear force response of the base isolation layer and first floor in the Y direction of ID5. As shown in the displacement time history, there was almost no displacement until 69 s, and the base isolation layer began to slide at 69 s. As shown in the time-history layer shear force response up to 69 s, the shaking table and first floor are subjected to the same acceleration until the spherical sliding bearing starts to slip; thus, the story shear force increases on both the first and second floors according to the shaking table acceleration. As the behaviors of the base isolation layer and the first layer are different during sliding after 69 s, the mass of the first floor affects the story shear forces of the base isolation layer, and the first layer mutually, and the story shear force of the first layer is larger than that of the base isolation layer. Therefore, the seismic isolation layer reached its maximum value at approximately 23 s before sliding, owing to the effect of the static friction coefficient.

In comparison, the first floor reached its maximum shear force at approximately 81 s during sliding, which was unaffected by the static friction coefficient. Regarding the response spectrum, the acceleration response spectrum of OS2_50% (Figure 4C) had a maximum acceleration of approximately 0.1G (G is the gravitational acceleration) for the natural period range of 4 to 6 s. The maximum static friction coefficient of this isolation unit test shown in Figure 9 is $\mu_{smax} = 0.059$. Therefore, the effect of the static friction coefficient on the maximum shear force acting on the superstructure was considered small compared to the design shear.

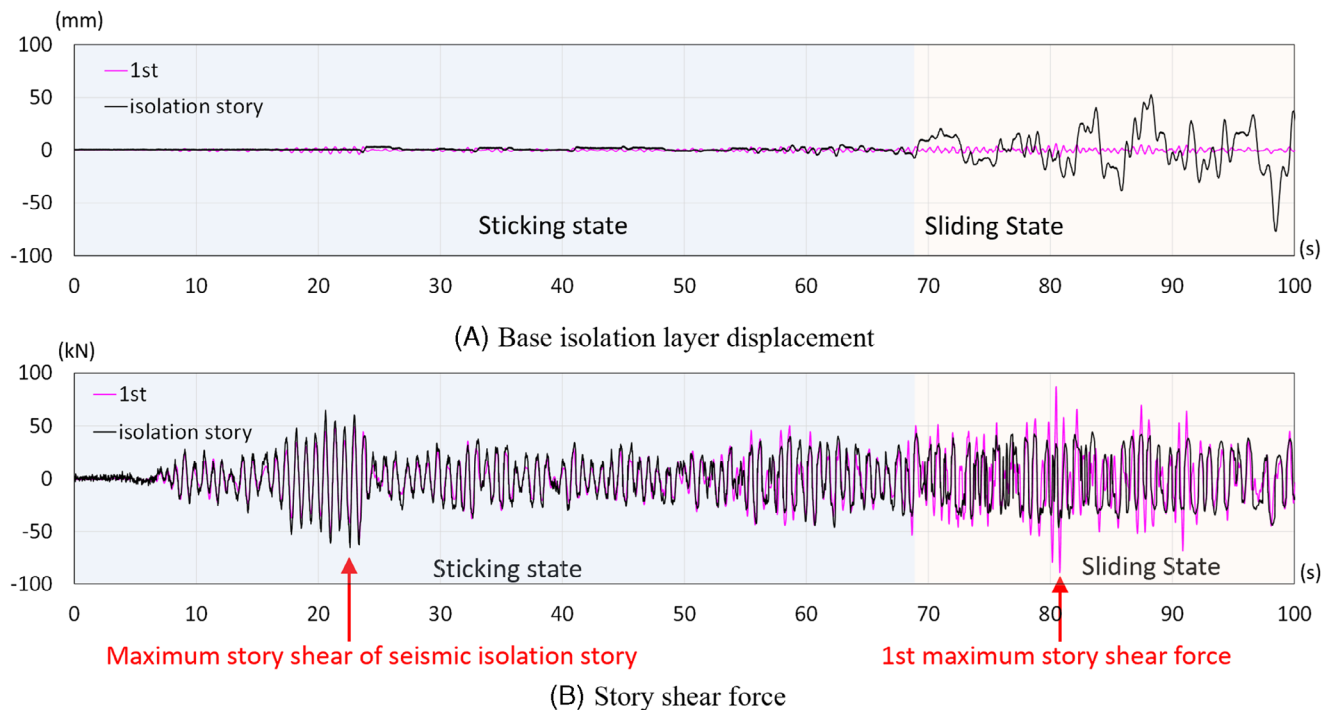


FIGURE 13 ID5-Y directional time history (experimental results).

TABLE 6 Varying axial force of seismic isolation materials.

	Loading											
	ID4				ID5				ID6			
SSB no.	No. 1	No. 2	No. 3	No. 4	No. 1	No. 2	No. 3	No. 4	No. 1	No. 2	No. 3	No. 4
Varying axial force ratio	0.15	0.14	0.17	0.12	0.34	0.09	0.10	0.34	0.63	0.60	0.55	0.66

4.5 | Low contact pressure

This section investigates the effects of fluctuating axial force and vertical motion input on the behavior of the base isolation layer using numerical analysis and experimental results. Note that the specimen had an aspect ratio of approximately two. A MDOF model common in design was adopted for numerical simulations. The input motions considered were ID4 and ID5, cases for large earthquakes, and ID6, cases for large earthquakes that exceed the design level and include vertical motions.

4.5.1 | Axial force variation

Table 6 lists the fluctuating axial forces of seismic isolation systems ID4, ID5, and ID6. The fluctuating axial force was approximately 15% of the long-term axial force for ID4 and approximately 30% for ID5. In the case of ID6, which considered vertical motion, approximately 60% of the variable axial force was generated, indicating that the magnitudes of the variable axial force and vertical motion were not small. The comparison between the experimental and numerical analysis results of the MDOF model, while neglecting the fluctuating axial force for the ID4 direction input in Figure 14, indicates that the effect of the variable axial force is negligible for the unidirectional input, as the story shear force, displacement, and velocity all correspond well.

4.5.2 | Diagonal (45°) and vertical input

Figure 15A,B compare the numerical analysis and experimental results of the MDOF model, ignoring the fluctuating axial force at the ID5 direction input. In (A), the shaking table acceleration in the X direction was used as the unidirectional

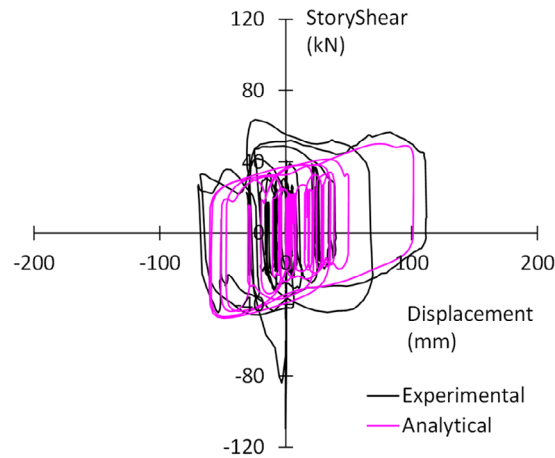


FIGURE 14 Hysteresis characteristics of base isolation (ID4).

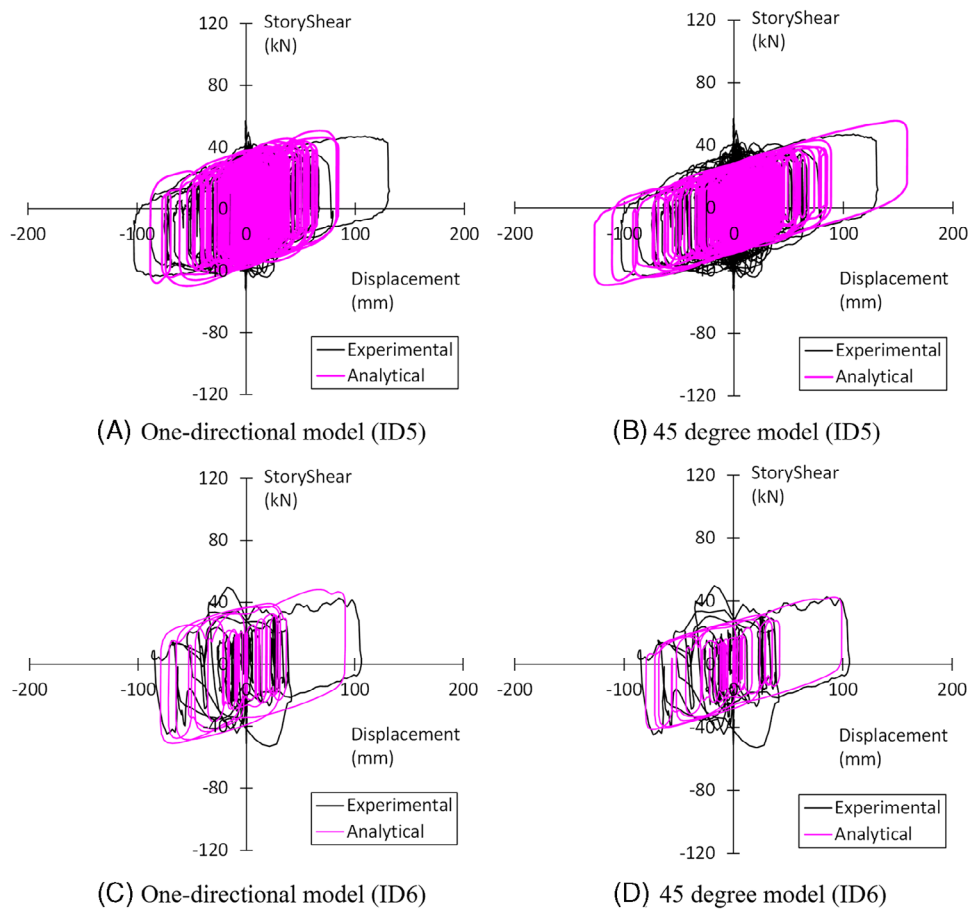


FIGURE 15 Comparison of simulation results against x-axis projected responses.

input. In (B), the input acceleration was multiplied by the square root of two to account for the XY 45-degree input, and the responses were divided by the square root of two to obtain the responses in each direction. Note that XY 45-degree input was planned to evaluate primarily the behavior of the fixed-based specimen.

As the equivalent stiffness of the spherical sliding bearing decreases as the absolute displacement increases, (A) with a unidirectional input underestimates the response displacement, whereas (B) shows good agreement with the experiment. The spherical sliding bearing has infinite stiffness until it starts sliding, exhibiting a low stiffness corresponding to the dynamic friction coefficient during sliding. In other words, the equivalent eigenfrequency fluctuates from time to

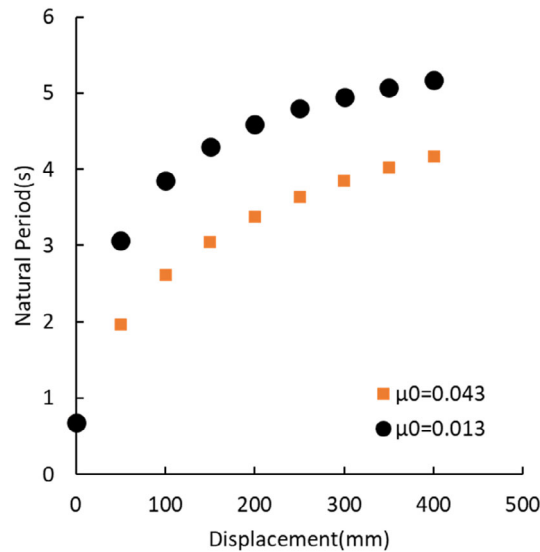


FIGURE 16 Relationship between seismic isolation displacement and equivalent natural period.

time depending on the displacement, and the nonlinearity owing to the displacement is strong enough to influence the responses.

Figure 15C,D compare the numerical analysis results and experimental results of the MDOF model, ignoring the varying axial force and vertical motion when the input was in ID6. The responses match well in both (C) and (D). These results suggest that the behavior of a seismically isolated low-rise building using a spherical sliding bearing can be predicted well with the MDOF model that ignores the effects of fluctuating axial force and vertical motion.

4.6 | Responses with low and moderate friction coefficients

Figure 16 shows the eigenvalue analysis results for SSBs with low and moderate friction coefficients. The equivalent natural periods were calculated using the secant stiffness of the isolation layer. The equivalent natural period with a moderate friction coefficient is less than 3.0 s up to a response displacement of 15 cm or less. This indicates that the stiffness is high in the small-displacement region, and acceleration tends to increase. Therefore, in an actual design, it is considered effective to use low-friction spherical sliding bearings to suppress acceleration and absorb energy using dampers with low initial stiffness, such as U-shaped dampers,²⁴ to reduce displacement.

With a dynamic friction coefficient of 0.013, the maximum floor response acceleration was less than 200 cm/s², and the maximum floor response velocity was less than 30 cm/s for all low-friction spherical sliding bearings in the experimental results (Table 5). Table 7 lists the numerical analysis results when the dynamic friction coefficient is 0.043, which is also available for SSB. The displacement of the isolation layer decreased when the friction coefficient increased, but the acceleration and velocity increased, with a maximum floor response acceleration of approximately 350 cm/s² and a maximum floor response velocity of approximately 70 cm/s for the ID6 input earthquake motion. Note that the maximum response acceleration, velocity, and displacement are shown for the 45° excitation when the input acceleration is multiplied by the square root of two using a mass-point system model.

In the fixed-based specimen connected to the base-isolated specimen (Figure 3A), the medical equipment around the bed moved approximately 30 cm at an acceleration of 350 cm/s² and a velocity of 50 cm/s, confirming the need to suspend treatment during vibration, and an IV stand overturned at an acceleration of 400 cm/s² and a velocity of 60 cm/s, as shown in Figure 17.²⁵ Thus, when all the bearings are moderate-friction bearings, the disorder will appear, unlike low-friction bearings. The effect of low-friction spherical sliding bearings in reducing damage to indoor medical equipment can be confirmed.

Figure 18 depicts the floor acceleration spectra and the energy spectra of the floor acceleration. First, with a low friction coefficient, there are no significant peaks in the acceleration spectra, while the energy spectra peaked in the first natural period. The difference between the long-period, long-duration earthquake motion (ID3) and short-period pulse-type ground motion (ID4) became more significant with the energy spectrum. The amplification ratios from the ground to the

TABLE 7 Maximum responses, $\mu_0 = 0.043$.

Peak floor acceleration (PFA, unit: cm/s^2)						
ID	1	2	3	4	5	6
3rd Floor	186	176	179	312	297	362
2nd Floor	119	126	138	253	272	289
1st Floor	110	117	78	197	153	217
Table	120	136	74.5	357	283	529
Peak floor velocity (PFV, unit: cm/s)						
3rd Floor	14.6	15.1	13.1	46.0	32.8	64.3
2nd Floor	12.3	13.5	8.4	47.9	30.7	67.0
1st Floor	11.1	12.3	6.8	40.0	31.9	57.7
Table	14.9	15.0	10.1	45.9	31.5	63.2
Base isolation layer response displacement (unit: cm)						
1st Floor	1.47	1.83	2.00	6.52	9.43	13.9

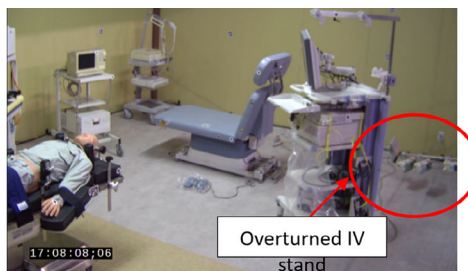
(A) Base-isolated (PFA = 92 cm/s^2 , PFV = 17 cm/s)(B) Fixed-base (PFA = 400 cm/s^2 , PFV = 60 cm/s)

FIGURE 17 Photos after ID4 loading.

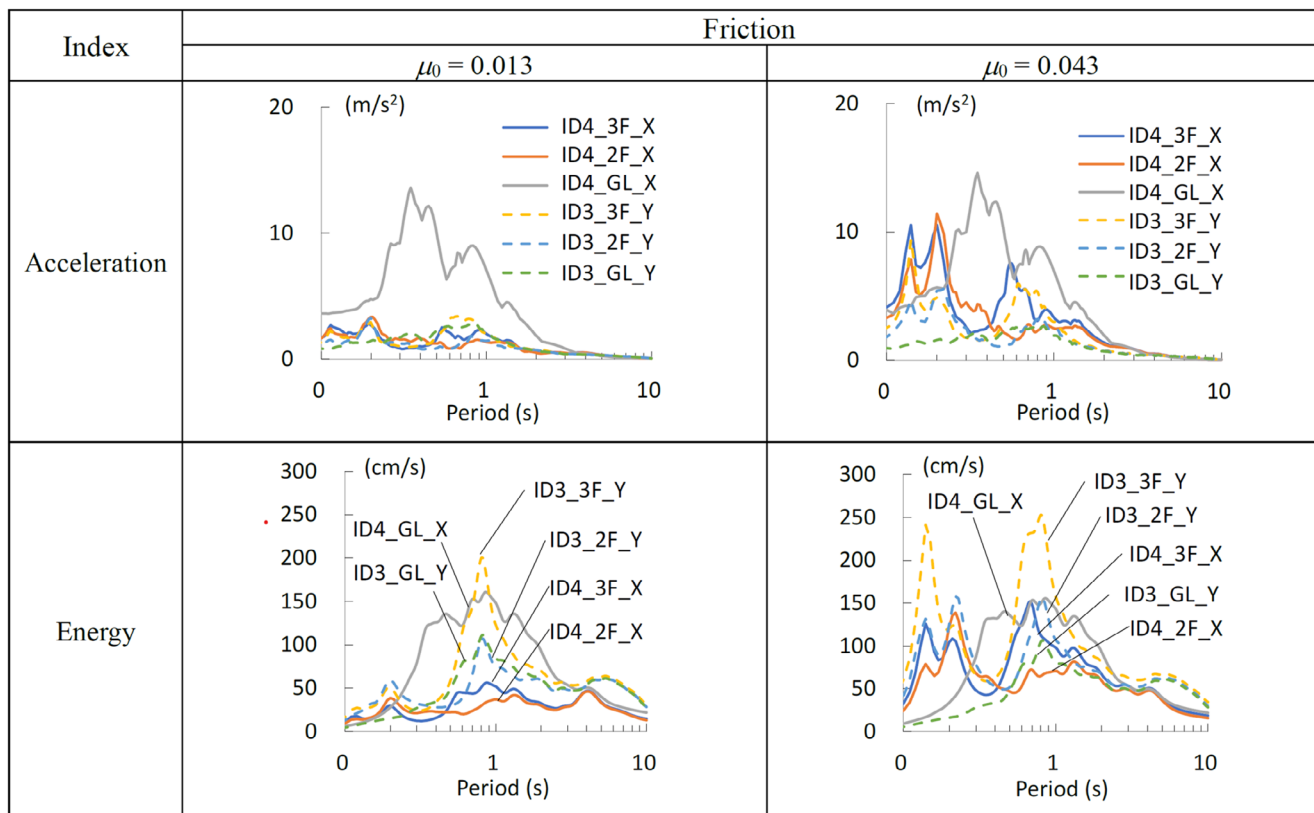


FIGURE 18 Floor response spectrum.

floor responses are larger for ID3 than ID4. As a result, even if the maximum floor response acceleration is larger for ID4, the peak values of the floor acceleration response spectrum and energy spectrum are larger for ID3. Second, with a moderate friction coefficient, the peaks at the small period range become significant. In particular, the impact of long duration becomes significant in the energy spectra at both the short period range and the natural period of building. According to previous research,²⁵ the displacement of medical equipment largely depends on the duration of ground motions and thus the floor energy spectra. Thus, the damage in the hospital room may be considerably larger with a moderate friction case and a long-period, long-duration earthquake motion.

5 | CONCLUSIONS

This study reported the results of a full-scale shake table testing of a base-isolated hospital building using spherical sliding bearings and the associated prediction by a simple method and numerical simulation used in design practice. The paper also discussed simulation methods with good prediction accuracy and the preferable performance of base isolation devices for reducing hospital disorders. The major findings are as follows:

- The response spectrum method overestimated the maximum displacement in the test for a long-period and long-duration earthquake motion. The response was generally good for near-fault ground motion with a relatively short-period pulse.
- In the blind prediction contest, the average error on the roof acceleration peaks over the test is around 65%–93% depending on test IDs, while the error on the isolation displacement is 17%–28%. The top-performing team had 10.3% and 8.9% errors for roof acceleration and isolation displacement using OpenSees with the singleFPBearing element.
- In sensitivity analysis, a velocity-dependence equation of the dynamic friction coefficient for low-friction sliding bearings required modification for low contact pressure and low-velocity conditions. The effects of axial force fluctuation and vertical motion were also minor regarding overall responses.
- The static friction coefficient identified in the shake table test was 1.9 to 4.5 times higher than the dynamic coefficient, and its average was about 2.3 times the isolation unit testing result of 0.0179 (at a velocity of 400 mm/s). Still, the effect on the residual displacement, cumulative travel, and the maximum shear force in the superstructure was small. The results with limited influence support the current design process that ignores the static friction coefficient.
- A low-friction spherical sliding bearing with a dynamic coefficient of friction of 0.013 significantly reduced the acceleration and velocity, thereby limiting damage to internal medical equipment in the test. With a friction coefficient of 0.043, the energy floor response spectrum increased significantly for the long-period, long-duration earthquake motion. The increase may cause disorder in a hospital room with displaced medical equipment.

In an actual design, it is considered effective to use low-friction spherical sliding bearings to suppress acceleration and absorb energy using dampers with low initial stiffness, such as U-shaped dampers, to reduce displacement. Combining low- and moderate-friction bearings to achieve target values in floor acceleration and isolation layer displacement is also common.

ACKNOWLEDGMENTS

We are grateful to Nippon Steel Corporation, Nittetsu Kenzai, Nittetsu Engineering, SENQCIA, Niitaka Corp, CentralUni, Nikkiso, Tajima Roofing, Morimatsu Kogyo, Naito Design, and OKUJU for their cooperation in the design and fabrication of the test specimens and to the students, technical staff, and medical staff of Kyoto University Hospital, Uji Tokusyukai Hospital, Nishijin Hospital, Kosei Hospital, and Ogaki Municipal Hospital for their efforts in preparing and conducting the experiments. We would like to thank Prof. Takashi Tanii of Waseda University and Mr. Takashi Kaneko of Kajima Corporation for their cooperation with the story drift measurements and Ms. Jasmine Gipson and Dr. Liangjie Qi for helping the blind prediction contest. This research was supported by the Tokyo Metropolitan Resilience Project of the National Research Institute for Earth Science and Disaster Resilience (NIED) (Subject C-3 leader: Masahiro Kurata). The financial support from the Japan Society for the Promotion of Science (Grant No. JP21H04598) is highly appreciated.

DATA AVAILABILITY STATEMENT

The data that support the findings of this study are available from the corresponding author upon reasonable request.

ORCID

Masahiro Kurata  <https://orcid.org/0000-0003-1624-1127>

REFERENCES

1. Cabinet Office Website: Nankaitorafu Jishinbosai Taisaku (Nankai Trough earthquake disaster prevention measures). (in Japanese). <https://www.bousai.go.jp/jishin/nankai/>
2. Achour N, Miyajima M. Post-earthquake hospital functionality evaluation: the case of Kumamoto earthquake 2016. *Earthq Spectra*. 2020;36(4):1670-1694.
3. Sato E, Furukawa S, Kakehi A, Nakashima M. Full-scale shaking table test for examination of safety and functionality of base-isolated medical facilities. *Earthq Eng Struct Dyn* 2011;40(13):1435-1453.
4. Kawabe H, Kaname K, Irikura K, Damage prediction of long-period structures during subduction earthquakes-Part 1: long-period ground motion prediction in the Osaka basin for future Nankai earthquakes. In: *The 14th World Conference on Earthquake Engineering*. 2008.
5. Nakagawa Y, Kaname K, Kawabe H, Irikura K, Damage prediction of long-period structures during subduction earthquakes-Part 2: long-period ground motion prediction in the Osaka basin for future Nankai earthquakes. In: *The 14th World Conference on Earthquake Engineering*. 2008.
6. Chung Y, Nagae T, Fukuyama K, et al. Seismic resistance capacity of high-rise buildings subjected to long-period ground motions-E-Defense shaking table test. In: *The 14th World Conference on Earthquake Engineering*. 2008.
7. Chung Y, Nagae T, Hitaka T, Nakashima M. Seismic resistance capacity of high-rise buildings subjected to long-period ground motions: E-Defense shaking table test. *J Struct Eng*. 2010;136(6):637-644.
8. The Architectural Institute of Japan (AIJ): Structural response and performance for long period seismic ground motions, 2007. (in Japanese).
9. Quaglino V, Dubini P, Poggi C. Experimental assessment of sliding materials for seismic isolation systems. *Bull Earthquake Eng*. 2012;10:717-740.
10. Lomiento G, Bonessio N, Benzoni G. Friction model for sliding bearings under seismic excitation. *J Earthq Eng*. 2013;17:1162-1191.
11. Quaglino V, Bocciarelli M, Gandelli E, Dubini P. Numerical assessment of frictional heating in sliding bearings for seismic isolation. *J Earthq Eng*. 2014;18:1198-1216.
12. Kumar M, Whittaker AS, Constantinou MC. Characterizing friction in sliding isolation bearings. *Earthq Eng Struct Dyn*. 2015;44:1409-1425.
13. Bianco V, Bernardini D, Mollaioli F, Monti G. Modeling of the temperature rises in multiple friction pendulum bearings by means of thermomechanical rheological elements. *Arch Civ Mech Eng*. 2018;19:171-185.
14. Zayas VA, Low SS, Mahin SA. A simple pendulum technique for achieving seismic isolation. *Earthq Spectra*. 1990;6(2):317-333.
15. Bao Y, Becker TC, Hamaguchi H. Failure of double friction pendulum bearings under pulse-type motions. *Earthq Eng Struct Dyn*. 2017;46:715-732. doi:10.1002/eqe.2827
16. Constantinou M, Mokha A, Reinhorn A. Teflon bearings in base isolation II: modeling. *J Struct Eng*. 1990;116(2):455-474.
17. Nishimoto K, Wakita N, Hasegawa H, Nakamura S, Full-scale Performance Verification Test of Spherical Surface Sliding Bearing (SSB) Low Friction Type (AIJ), 2017. (in Japanese).
18. Barone S, Calvi GM, Pavese A. Experimental dynamic response of spherical friction-based isolation devices. *J Earthq Eng*. 2019;23(9):1465-1484.
19. Konishi Y, et al. A Study on the Response Characteristics of a Seismic Isolated Building with Spherical Sliding Bearing (SSB) in the Wind Direction (AIJ). 2020 (in Japanese).
20. NIPPON STEEL ENGINEERING. NS-SSB Catalog. https://www.eng.nipponsteel.com/steelstructures/wp/wp-content/uploads/2022/08/NS-SSB_202207.pdf
21. Building Research Institute: Technical Background of Regulations Related Seismic Isolation in Revised Building Standards Law. 2001. 8 (in Japanese)
22. Commentary on Structural Regulations of the Building Standard Law of Japan Editorial Committee. 2020. 11.
23. The Japan Society of Seismic Isolation: Maintenance Standards for Seismically Isolated Buildings. 2018 (in Japanese).
24. Kishiki S, Ohkawara Y, Yamada S, Wada A. Experimental evaluation of cyclic deformation capacity of U-shaped steel dampers for base-isolated structures. *J Struct Constr Eng AIJ*. 2008;73(624):333-340. 2 (in Japanese).
25. Kurata M, Akazawa M, Aida S, et al. Seismic behavior of medical equipment in earthquake-resistant and seismically-isolated buildings at e-defense shaking table tests. *J Struct Constr Eng AIJ*. 2023;88(809):1116-1123. (in Japanese).

How to cite this article: Akazawa M, Kurata M, Yamazaki S, Kawamata Y, Matsuo S. Test and sensitivity analysis of base-isolated steel frame with low-friction spherical sliding bearings. *Earthquake Engng Struct Dyn*. 2024;1-19. <https://doi.org/10.1002/eqe.4249>